

PCCP

Accepted Manuscript



This is an *Accepted Manuscript*, which has been through the Royal Society of Chemistry peer review process and has been accepted for publication.

Accepted Manuscripts are published online shortly after acceptance, before technical editing, formatting and proof reading. Using this free service, authors can make their results available to the community, in citable form, before we publish the edited article. We will replace this *Accepted Manuscript* with the edited and formatted *Advance Article* as soon as it is available.

You can find more information about *Accepted Manuscripts* in the [Information for Authors](#).

Please note that technical editing may introduce minor changes to the text and/or graphics, which may alter content. The journal's standard [Terms & Conditions](#) and the [Ethical guidelines](#) still apply. In no event shall the Royal Society of Chemistry be held responsible for any errors or omissions in this *Accepted Manuscript* or any consequences arising from the use of any information it contains.

Seurchin-like hierarchical NiCo₂O₄@NiMoO₄ core/shell nanomaterials for high performance supercapacitor

Qiang Zhang, Yanghua Deng, Zhonghua Hu*, Yafei Liu, Mingming Yao, Peipei Liu, Department of Chemistry, Tongji University, 1239 Siping Road, Shanghai 200092, China

*Corresponding author. Tel.: +86 21 65982594, Fax: +86 21 65982594
E-mail address: huzh@tongji.edu.cn

Abstract: A novel electrode material of three-dimensional (3D) multicomponent oxide NiCo₂O₄@NiMoO₄ core/shell was synthesized via a facile two-step hydrothermal method with a post annealing procedure. The uniform NiMoO₄ nanosheets were grown on the seurchin-like backbone NiCo₂O₄ to form NiCo₂O₄@NiMoO₄ core/shell materials constructed by interconnected ultrathin nanosheets, so that to produce hierarchical mesopores with a large specific surface area of 100.3 m² g⁻¹. The porous feature and core/shell structure can facilitate the penetration of electrolytic ions and increases the amount of electroactive sites. Hence, the NiCo₂O₄@NiMoO₄ materials exhibited a high specific capacitance of 2474 F g⁻¹ and 2080 F g⁻¹ at current densities of 1 A g⁻¹ and 20 A g⁻¹ respectively, suggesting that it not only has a very large specific capacitance, but also a good rate performance. In addition, the capacitance lost only 5.0% after 1000 cycles of charge and discharge test at the current density of 10 A g⁻¹, indicating high stability. The excellent electrochemical performance is mainly attributed to its 3D core/shell and hierarchical mesoporous structures which can provide unobstructed pathways for the fast diffusion and transportation of ions and electrons, a large number of active sites and good strain accommodation.

Keywords: NiCo₂O₄@NiMoO₄, seurchin-like, core/shell structure, supercapacitor,

hydrothermal method

1. Introduction

Developing sustainable and renewable energy is one of the most important tasks for scientists and engineers worldwide to address the rapidly increasing global energy consumption, coupled with the critical issue of climate change [1-5]. Electrochemical capacitors (ECs) are widely investigated due to their interesting characteristics of high power density, fast charging capability, exceptional cycle life, high coulombic efficiency and safety [6-10]. As complementary or substituting power source for rechargeable batteries and fuel cells, ECs have been used in many applications, such as electric vehicles, power back-up and pacemakers [11].

As a typical metal oxide electrode material for ECs, ruthenium oxide has shown the best performance [12]. However, it is hardly to be commercialized due to the high cost.[13] To date, many efforts have been devoted to find cost-effectively alternative transition metal oxides with good capacitive characteristics, especially those possess multiple oxidation states/structures that enable rich redox reactions such as metal oxides MnO_2 [14, 15], NiO [16, 17], Co_3O_4 [18, 19], etc. Nickel-cobalt metal oxide has drawn intensive research attention because it has a high theoretical capacitance, and it is low-cost, abundant and environmental-friendly. Besides, it is expected to offer richer redox reactions, including contributions from both nickel and cobalt oxides, than that of two corresponding single-component oxides [20]. However, transition metal oxides including NiCo_2O_4 usually showed limited kinetics during the redox reaction due to their low electrical conductivity and low surface area[21]. Interestingly, metal molybdates like NiMoO_4 possesses a high specific capacitance, owing to the high electrochemical activity of nickel ion, but its rate performance is poor[22].

Recently, the research on the complex heterostructured nanomaterials is a hot topic. These heterostructured complexes show higher electrochemical performance than mono-metal oxides. Mai et al. reported that the hierarchical-pores nanowires of heterostructured $\text{MnMoO}_4/\text{CoMoO}_4$ have a specific capacitance of 187.1 F g^{-1} at a current density of 1 A g^{-1} with a cycling efficiency of 98% after 1,000 cycles, and are

superior to mono-metal oxide of MnO_2 or Co_3O_4 [23]. The hetero-nanostructured $\text{NiCo}_2\text{O}_4@\text{NiCo}_2\text{O}_4$ and $\text{NiCo}_2\text{O}_4@\text{NiO}$ at 0.5 A g^{-1} demonstrate excellent electrochemical performance with high specific capacitance (1925 and $2210 \text{ F} \cdot \text{g}^{-1}$, respectively), good rate capability, and superior cycling stability than pure NiCo_2O_4 [24]. Various heterostructured materials showed superior electrochemical performance owing to their synergistic effects [22-25].

In the present work, a novel heterostructured $\text{NiCo}_2\text{O}_4@\text{NiMoO}_4$ core/shell electrode material was designed. Because both individual salts NiMoO_4 and NiCo_2O_4 them-self are promising candidate materials for supercapacitors, the combination of the two materials to form sophisticated core/shell structure is expected to enhance greatly the surface area to provide more electroactive sites for Faradaic reactions and create fast pathways for electrolytic ions and electrons' diffusion and transportation, and enabling synergistical effect of NiCo_2O_4 and NiMoO_4 , so that improve significantly the electrochemical performance of the heterostructured material. The strategy is to deposit NiMoO_4 nanospecies outside of the NiCo_2O_4 nanoparticles to form core/shell heterostructure. Therefore a two-step approach of hydrothermal synthesis and calcination was proposed. NiCo_2O_4 was prepared as "core"; than NiMoO_4 was deposited as "shell".

2. Experimental

2.1. Preparation of $\text{NiCo}_2\text{O}_4@\text{NiMoO}_4$ Composite

All reagents are of analytical grade and were purchased from Sinopharm Chemical Reagent Co. Ltd and used without any purification.

(1) Synthesis of NiCo_2O_4 : In a typical synthesis, 1 mmol of $\text{NiCl}_2 \cdot 6\text{H}_2\text{O}$, 2 mmol of $\text{CoCl}_2 \cdot 6\text{H}_2\text{O}$ and 12 mmol urea were dissolved in 80 mL deionized (DI) water under constant magnetic stirring to form a transparent pink solution. The solution was transferred to a 100 mL Teflon-lined stainless steel autoclave; the hydrothermal reaction was carried out at 120°C for 12 h . After the reactor cooled to room temperature, the product was collected, washed, vacuum-dried, and calcinated at 300°C in air atmosphere for 3 h , then moved into an oven at 60°C for 12 h .

(2) Synthesis of NiCo₂O₄@NiMoO₄ hybrid material: The NiMoO₄ was on the prepared NiCo₂O₄ to form NiCo₂O₄@NiMoO₄ material by hydrothermal method too. 0.25 g of above synthesized NiCo₂O₄ was dispersed in 80 ml deionized water with ultrasonic stirring for 10 min. Then, 2 mmol of NiSO₄·7H₂O and 2 mmol Na₂MoO₄·7H₂O was added, the mixture was kept under ultrasonic stirring for 5 minutes and then transferred to a 100 mL Teflon-lined stainless steel autoclave, and heated to 120°C for 12h. After cooling down to room temperature, the products were taken out and rinsed with deionized water and alcohol several times, then dried at 60°C for 12 h.

2.2. Characterization

The prepared sample was examined by X-ray diffraction (XRD; D8, Bruker), field emission scanning electron microscope (FESEM; XL30, Philips), and high-resolution transmission electron microscope (HRTEM; JEM-2100, JEOL) and N₂ adsorption (Micromeritics, Tristar 3000 gas adsorption analyzer).

2.3. Electrochemical Measurements

A three-electrode cell was used for electrochemical measurements with as-prepared samples as the working electrode, and a nickel mesh and Hg/HgO as the counter and reference electrodes, respectively. 6 M KOH solution was used as electrolyte. The working electrode containing 2-3 mg active materials were prepared by mixing active materials, carbon black and polytetrafluoroethylene (PTFE) in a mass ratio of 8:1:1. A small amount of ethanol was added into the mixture to form a paste and pressed into a sheet of about 1 mm in thickness, then, a small wafer of 10 mm in diameter is cut off with a hole puncher to obtain electrodes, which is pressed by bead machine under 10 MPa on Ni mesh substrate to form the working electrodes. The working electrode was impregnated with the electrolyte for 30 min to ensure the nanocomposite electrode

was thoroughly wet and then activated with a small current with chronopotentiometry. The electrochemical measurements were performed on a CHI660C electrochemical workstation (Chenhua, Shanghai). The specific capacitance is calculated according to the following equation:

$$C_p = \frac{I\Delta t}{m\Delta V} \quad (1)$$

Where $C(\text{F}\cdot\text{g}^{-1})$ is the specific capacitance, I (A) represents the discharge current, and $m(\text{mg})$, $\Delta V(\text{V})$, and Δt (s) designates the mass of active materials, potential drop during discharge, and total discharge time respectively.

3. Results and discussion

3.1 Formation mechanism of NiCo₂O₄@NiMoO₄ core/shell nanomaterials

The formation mechanism of NiCo₂O₄@NiMoO₄ core/shell nanomaterials was presumed as shown in Scheme 1. Firstly, Seurchin-like nano-NiCo₂O₄ cores were prepared. Second, a thin layer of NiMoO₄ was coated onto the surface of the NiCo₂O₄ core to form the final products of hierarchical NiCo₂O₄@NiMoO₄ core/shell nanomaterials.

3.2 Physicochemical Characterization.

TG and DTG measurements were performed to assess the follow-up calcination process of the as-prepared NiCo₂O₄ precursors. As depicted in Fig. 1a, the sample undergoes a weight loss of 24.18% in the multistep weight loss process involving the dehydration and decomposition of precursors. The weight loss (1.4%) below 150°C is ascribed to the removal of adsorbed water and the evaporation of the intercalated water molecules.[26]The subsequent weight loss (21.8%) with a strong endothermic peak at 250–300 °C arises from the loss of water and CO₂ generated by the dehydroxylation and decomposition of precursors.[27] At 300 °C, almost all the intercalated water molecules and gas molecules escaped from the interslab space

completely, leading to the formation of porous spinel NiCo_2O_4 . At higher temperature, no obvious weight loss is observed indicating that there is no additional phase or structural change in NiCo_2O_4 . Therefore, in order to obtain the NiCo_2O_4 with high purity, 300 °C is chosen as the calcination temperature.

The crystal structures of as-synthesized NiCo_2O_4 , NiMoO_4 and $\text{NiCo}_2\text{O}_4@\text{NiMoO}_4$ were studied by XRD as shown in Fig.1(b). The diffraction peaks at 18.9, 31.2, 36.7, 38.4, 44.6, 55.4, 59.1, 65.0° can be indexed as the (111), (220), (311), (222) (400), (422), (611) and (440) crystal planes of NiCo_2O_4 (JCPDS card no. 73-1702). The broad diffraction peaks indicate the poor crystallinity of the pristine NiCo_2O_4 . The patterns of single NiMoO_4 are in good agreement with the standard patterns for $\text{NiMoO}_4 \cdot x\text{H}_2\text{O}$ (JCPDS, card no. 13-0128). In addition, several diffraction peaks were attributed to the impurity phase of NiMoO_4 (JCPDS, card no. 12-0348). After the hydrothermal growth of the NiMoO_4 nanosheets, the pattern of $\text{NiCo}_2\text{O}_4@\text{NiMoO}_4$ contains the peaks of NiCo_2O_4 , NiMoO_4 (JCPDS, card no.12-0348) and $\text{NiMoO}_4 \cdot x\text{H}_2\text{O}$ (JCPDS, card no.13-0128), indicating two phase of as-synthesized NiMoO_4 are coexisted on the surface of NiCo_2O_4 . The intensity diffraction peaks corresponds to the NiCo_2O_4 reduced in the patterns of $\text{NiCo}_2\text{O}_4@\text{NiMoO}_4$ materials, probably due to the winding of NiMoO_4 nanosheets on the surface of the NiCo_2O_4 nanostructure and covering up by the strong diffraction peaks of NiMoO_4 .

In order to further understand the elemental composition and the oxidation state of as-prepared $\text{NiCo}_2\text{O}_4@\text{NiMoO}_4$, XPS measurements were carried out and the results are presented in Fig. 2. Fig. 2a indicates the presence of Ni, Mo, Co, and O as well as C from the reference and no other elements are detected. The Ni 2p core level spectrum (Fig. 2b) is reasonably deconvoluted into four peaks. The binding energy peak at 856.2 eV and its satellite peak at 861.9 eV correspond to Ni 2p_{3/2}, whereas, the binding energy peaks at 874 eV and its satellite peak at 879.8 eV correspond to the Ni 2p_{1/2} level. The main binding energy peaks of Ni 2p_{3/2} and Ni 2p_{1/2} are separated by 17.8 eV, which is a signature of the Ni²⁺ oxidation state.[28] The Mo 3d core level spectrum (Fig. 2c) shows two peaks with binding energies of 232.2 eV and 235.3 eV

corresponding to Mo 3d_{5/2} and Mo 3d_{3/2}, respectively. The binding energy peaks of Mo 3d are separated by 3.1 eV, which also signifies a Mo(VI) oxidation state.[29] In Co 2p spectra (Figure 2d), two kinds of Co species can also be observed and assigned to the species containing Co(II) and Co(III) ions.[30,31] Specifically, the fitting peaks at binding energies (EB) of Co(II) ions at 781.7 and 796.9 eV are attributed to Co²⁺, while the other two fitting peaks at 780.1 and 795.2 eV belong to Co³⁺ and two shakeup satellites (identified as “Sat.”). The high-resolution spectrum for the O 1s region (Figure 5d) shows three oxygen contributions. Specifically, the peak at 530.2 eV is typical of metal–oxygen bonds.[30,31] The peak sitting at 531.4 eV is usually associated with defects, contaminants, and a number of surface species including hydroxyls, chemisorbed oxygen, under-coordinated lattice oxygen, or species intrinsic to the surface of the spinel.[32] The peaks at 532.6 eV can be attributed to multiplicity of physi- and chemisorbed water at or near the surface.[30,31] These results show that the surface of the as-synthesized NiCo₂O₄@NiMoO₄ materials has a composition containing Ni²⁺, Ni³⁺, Mo(VI), Co²⁺, Co³⁺ and O²⁻, which is in good agreement with the results of NiMoO₄ and NiCo₂O₄. Here, the surface quantitative analysis of the NiCo₂O₄@NiMoO₄ materials based on the XPS were also conducted, which displays that the surface Ni/Mo/O atomic ratio of the materials is 1.06/0.85/4.25, which is close to 1/1/4 for the stoichiometric NiMoO₄. The surface Co atomic percentage of the materials is only 1.51%, indicating that most of the surface materials are NiMoO₄ with only a few NiCo₂O₄. This result agrees well with the NiCo₂O₄@NiMoO₄ core/shell structure: NiCo₂O₄ was prepared as “core”; than NiMoO₄ was deposited as “shell”

Moreover, energy-dispersive X-ray spectrometry (EDS) spectrometry analysis was applied to further confirm the NiCo₂O₄@NiMoO₄ core/shell structure as shown in Fig.3. It is clear that it consist of Ni, Co, Mo and O elements and the nanosheets grown on the surface are mainly made of NiMoO₄ and the parent hierarchical heterostructures are a mixture of NiCo₂O₄ and NiMoO₄, which agrees well with the results of XRD.

The morphologies of the NiCo₂O₄ and NiCo₂O₄@NiMoO₄ were characterized by

FESEM as shown in Fig.4. The NiCo_2O_4 material has a seaurchin-like feature of 3-5 μm in diameter with sharp nano-needles emanated from the ball center, so that create large amount of open-free space in the balls as shown in Fig.4 (a) and (b). Fig.4(c,d) displays the SEM image of $\text{NiCo}_2\text{O}_4@ \text{NiMoO}_4$ core-shell materials. It is clear that the basic framework of NiCo_2O_4 is still retained, however, the needles of NiCo_2O_4 were uniformly wrapped by NiMoO_4 of short nanorods to form a core/shell nanostructure $\text{NiCo}_2\text{O}_4@ \text{NiMoO}_4$ nanomaterials, resulting in the formation of $\text{NiCo}_2\text{O}_4@ \text{NiMoO}_4$ bristled nanorods of about 200 nm in diameter. Furthermore, Fig 4(d) reveals that the covered nanorods outside of NiCo_2O_4 needles have pine leaves-like shape.

More details of the morphology and structure of the as-obtained NiCo_2O_4 and $\text{NiCo}_2\text{O}_4@ \text{NiMoO}_4$ core/shell nanomaterials are studied by TEM, HRTEM. Fig. 5a reveals that NiCo_2O_4 has the seaurchin-like structure with sharp nano-needles emanated from the ball center. It is well consistent with the FESEM observation. The lattice spacing of the (311) crystal plane of NiCo_2O_4 is 0.24 nm as shown by high-resolution TEM (HRTEM) image, Fig.5b. The nanorods $\text{NiCo}_2\text{O}_4@ \text{NiMoO}_4$ have a diameter about 200 nm (the edge of dark image) as shown in Fig.5c, it is in good agreement with that of SEM. The HRTEM image of the NiMoO_4 shell is displayed in Fig.5d. The interplanar spacing are of 0.31 nm and 0.35 nm, which are close to 0.312 nm and 0.35 nm given in the JCPDS 12-0348 file, the lattice spacing of 0.30 nm is close to that of 0.299 nm given in the JCPDS 13-0128 file. Unfortunately, the crystal structure of NiMoO_4 is not clear, it is still unknown which plane the obtained spacing corresponds to.

The N_2 adsorption-desorption isotherms and pore size distributions of the NiCo_2O_4 , NiMoO_4 and $\text{NiCo}_2\text{O}_4@ \text{NiMoO}_4$ coll/shell nanomaterials are shown in Fig. 6. It is clear that pure NiMoO_4 has a typical type II isotherm with a very low adsorbed amount at low relative pressures and a negligible desorption loop, indicating almost non-porous material; NiCo_2O_4 has a combination of Type II and IV isotherm with a very low adsorbed amount at low relative pressures and a small desorption loop, indicating the existence of a few mesopores; $\text{NiCo}_2\text{O}_4@ \text{NiMoO}_4$ has a typical Type

IV isotherm with a visible adsorbed amount at low relative pressures and a high adsorbed amount and a large desorption loop, indicating the existence of a large amount of mesopores as shown in Fig 6(a). Fig 6(b) show that NiMoO₄, NiCo₂O₄ and NiCo₂O₄@NiMoO₄ have a few pores located about 3 nm, a number of pores at about 7 nm and a large amount of pores at about 5 nm with some pores ranged from 10-23 nm, respectively, indicating that NiCo₂O₄@NiMoO₄ has hierarchical mesoporous characteristics.

The calculated BET specific surface areas, total pore volumes are given in Table 1. NiCo₂O₄@NiMoO₄ has the largest S_{BET} of 100.3 m²·g⁻¹, and V_{tot} of 0.241 cm³·g⁻¹ much higher than that of NiMoO₄ (39.2 m²·g⁻¹ 0.080 cm³·g⁻¹) and NiCo₂O₄ (42.2 m²·g⁻¹, 0.118 cm³·g⁻¹). The highly porosity and large surface of NiCo₂O₄@NiMoO₄ materials are attributed to the aggregation and gathering of NiMoO₄ nanorods grown on the NiCo₂O₄ needles to form hierarchical mesopores.

3.3. Electrochemical Measurements

Figure 7a shows the cyclic voltammetry (CV) curves of NiCo₂O₄, NiMoO₄ and NiCo₂O₄@NiMoO₄ electrodes at a scan rate of 10 mV s⁻¹. It is clear that the three electrodes display evidently a pair of redox peaks, i.e., oxidation peak at 0.26, 0.32, 0.27V and reduction peaks at 0.05, 0.11, -0.08 V for NiCo₂O₄, NiMoO₄ and NiCo₂O₄@NiMoO₄, respectively, which is mainly attributed to the redox reactions of Ni and Co species in the alkaline electrolyte[23,33-34].

The integral CV area and height of oxidation peak are in the order of NiCo₂O₄@NiMoO₄ > pure NiCo₂O₄ > NiMoO₄, indicating that the former electrode has a larger specific capacitance than the latter two. The core/shell nanoflake arrays have higher electrochemical reaction activity, it should be attributed to the additional pseudocapacitance contributed by the NiMoO₄ shell. It is in good agreement with that of the nitrogen adsorption and SEM observation. With a large surface area and porous structures, the as-synthesized NiCo₂O₄@NiMoO₄ nanomaterials have potential application in electrochemical supercapacitors since they may facilitate the ion transfer at the electrode/electrolyte interface[35]. Meanwhile, compared with that of

NiMoO₄, the area for the NiCo₂O₄@NiMoO₄ electrode obvious increase at the left side of the redox peaks. This increased area is mainly contributed by NiCo₂O₄. This means that both NiMoO₄ and NiCo₂O₄ are helpful to improve the supercapacitive performance of the NiCo₂O₄@NiMoO₄ electrode materials.

Fig. 7b shows the CV curves of the NiCo₂O₄@NiMoO₄ electrode at a scan rate of 2, 5, 10, 20 mV s⁻¹ in the potential range of - 0.2– 0.45 V (vs. SCE). It is evident that the peak current increases with increasing scan rate, suggesting that the kinetics of the interfacial and the rates of electronic and ionic transport are rapid enough at the scan rates presented. The anodic peaks shifted towards positive potential and the cathodic peaks shifted towards negative potential, which is attributed to the polarization effect of the electrode [36].

In order to get more information about the ability of the as-synthesized seurchin-like NiCo₂O₄@NiMoO₄ nanostructure electrodes, the galvanostatic charge–discharge tests were conducted at various charge–discharge current densities with the potential window between 0 and 0.35V, with a series of current densities up to 20 A g⁻¹ are presented in Fig.7c. A distinct plateau region can be observed during the process, suggesting the pseudocapacitive behavior of the electrodes. The specific capacitances at various discharge current densities for the three electrodes are calculated and shown in Fig.7d. At the current density of 1A g⁻¹, the specific capacitance of NiCo₂O₄@NiMoO₄ (2474F g⁻¹) are much larger than pristine NiCo₂O₄ (1471F g⁻¹) and NiMoO₄ (1228F g⁻¹). Although the specific capacitance gradually decreases with increasing current density due to the incremental voltage drop and that there is insufficient active material involved in the redox reaction at high current densities, the specific capacitance is still as high as 2080F g⁻¹ as the current density increase 20 times, from 1 to 20 A g⁻¹, implying that the NiCo₂O₄@NiMoO₄ electrode has super high rate charge-discharge performance. It is worth to mention that the specific capacitance of NiCo₂O₄@NiMoO₄ electrode of this work is also higher than that of other previously reported core/shell nanoarchitected materials, such as NiCo₂O₄@ graphene nanoarchitectures (778F g⁻¹ at 1 A g⁻¹) [37], and

NiCo₂O₄@NiCo₂O₄ (1917 F g⁻¹ at 1 A g⁻¹), NiCo₂O₄@NiO (2105 F g⁻¹ at 1 A g⁻¹) [24], Co/NiO core/shell nanowire arrays (956 F g⁻¹ At 2 Å g⁻¹) [38].

Fig.7e displays the EIS of NiCo₂O₄, NiMoO₄, and the hierarchical NiCo₂O₄@NiMoO₄ electrode. The inset shows the semicircle evident at high frequency. All the impedance spectra are similar, being composed of one semicircle at high frequency followed by a linear component at low frequency. There are two differences in these curves. Firstly, in the high frequency intercept of the real axis, the internal resistances (R_b) were different. Compared with NiMoO₄, the R_b of NiCo₂O₄@NiMoO₄ electrode was decreased, suggesting that the introduction of NiCo₂O₄ improved the electron conductivity of NiCo₂O₄@NiMoO₄. Secondly, the diffusive resistance (Warburg impedance) of the NiCo₂O₄@NiMoO₄ electrode, represented by the straight line at low frequency, was lower than that of NiMoO₄, indicating that the porous structure of the NiCo₂O₄@NiMoO₄ composite can reduce the mass-transfer resistance and enhance the electrolyte penetration as well as ion diffusion in the host material. What is more, the NiCo₂O₄@NiMoO₄ electrode also shows a small pseudo charge transfer resistance (R_{ct}), which corresponds to the small semicircle in the impedance plots. The low R_b , R_{ct} , and Warburg impedance reveal the excellent electrochemical capacitive properties of these binary metal oxide based composite materials.

The cycling stability of the NiCo₂O₄, NiMoO₄ and NiCo₂O₄@NiMoO₄ electrode were carried out at 10A g⁻¹ and the result are shown in Fig.7f. It is clear that the NiCo₂O₄, NiMoO₄ display a specific capacitance of 857F g⁻¹, 1170 F g⁻¹ and capacitance retention of 93.8% and 98%, respectively, after 1000 cycles at 10A g⁻¹. NiCo₂O₄@NiMoO₄ hybrid electrode has not only a good capacitance retention of 95%, but also exhibits a very high specific capacitance of 2148 F g⁻¹ after 1000 cycles.

In view of the high capacitance and excellent rate capability, we further calculate the specific energy and power densities, which are the two key factors for the practical applications of electrochemical supercapacitors. The specific energy density (E) and power density (P) are obtained based on the following equations, respectively:

$$E = \frac{1}{2} C \Delta V^2 \quad (2)$$

$$P = \frac{E}{\Delta t} \quad (3)$$

Where E is the specific energy density, C refers to the specific capacitance, ΔV is the voltage range, P represents the power density, and Δt is the discharge time. The results are presented as Ragone plots in Fig. 8. The NiCo₂O₄@NiMoO₄ sample can deliver high power output in the range of 175 and 3539 W kg⁻¹ with little sacrifice of the high energy density (from 42.1 to 35.4 Wh kg⁻¹). Whereas the other two samples exhibit slightly reduced but still quite impressive energy densities with the similar power densities. The excellent capability of delivering high specific power and energy densities makes the present mesoporous NiCo₂O₄@NiMoO₄ hierarchical structures very appealing as electrode materials for advanced supercapacitors.

The results demonstrate that NiCo₂O₄@NiMoO₄ core/shell nanomaterials electrode has excellent electrochemical performance reflected by an extreme large specific capacitance, low resistance, high cycling stability and capacitance retention, and good rate capability. All these merits are important for the practical application in supercapacitors.

4. Conclusions

A novel nanostructured core/shell NiCo₂O₄@NiMoO₄ hybrid was successfully synthesized through a facile two-step hydrothermal method free of templates and catalysts. The NiCo₂O₄@NiMoO₄ electrode exhibits good electrochemical performance with an extreme large capacitance of 2474 F g⁻¹ at 1A g⁻¹. At the high current density of 20 A/g, it still possesses 2080 F g⁻¹, indicating a good rate capability. It also exhibits a high capacitance retention of 95% after 1000 cycles of charge-discharge, suggesting a high recycle stability. The excellent electrochemical performance indicates that the integration of two metal oxides into one sophisticated core/shell hybrid nanostructure that is directly aligned on the current collector significantly enhances the areal capacitance. The results demonstrate that the NiCo₂O₄@NiMoO₄ core/shell electrode material would have a great application

potential in the electrochemical energy storage for supercapacitors.

5. Acknowledgements

This work is supported by Tongji University Research Foundation (1380219039). The authors would like to thank the workers from the Chemistry Experimentation Center of Tongji University and laboratory members for their help.

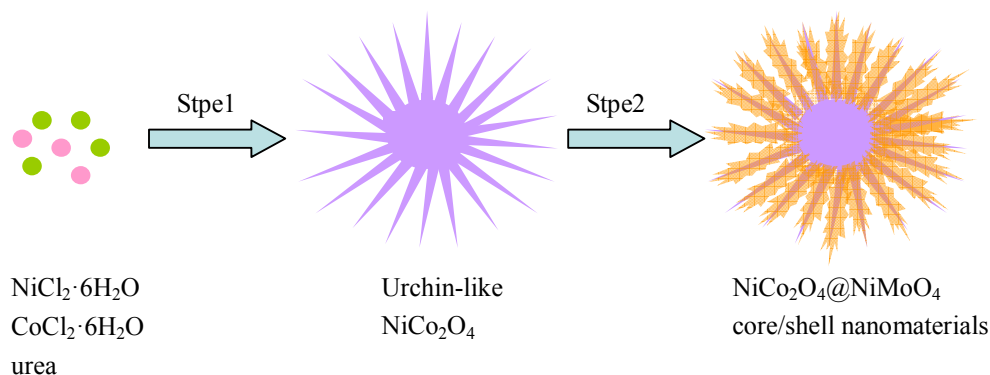
REFERENCES

- [1]. G. H. Yu, L. B. Hu, M. Vosgueritchian, H. L. Wang, X. Xie, J. R. McDonough, X. Cui, Y. Cui, Z. N. Bao, *Nano Lett* 11 (2011) 2905-2911.
- [2]. H. L. Wang, Y. Yang, Y. Liang, J. T. Robinson, Y.G. Li, A. Jackson, Y. Cui, H. Dai, *Nano Lett* 11 (2011) 2644-2647.
- [3]. S. Park, S. Jayaraman, *MRS Bull* 28 (2003) 585-591.
- [4]. J. Chmiola, C. Largeot, P. L. Taberna, P. Simon, Y. Gogotsi, *Science*. Washington. DC. U. S 328 (2010) 480-483.
- [5]. J. Tollefson, *Nature*. London. U. K 456 (2008) 436-440.
- [6]. L. Buglione, M. Pumera, *Electrochem. Commun* 17 (2012) 45-47.
- [7]. K. H. Jung, W. Deng, D. W. Smith, J. P. Ferraris, *Electrochem. Commun* 23 (2012) 149-152.
- [8]. C. Z. Yuan, L. Yang, L. R. Hou, L. F. Shen, X. G. Zhang, X. W. Lou, *Energ. Environ. Sci* 5 (2012) 7883-7887.
- [9]. P. C. Chen, G. Shen, Y. Shi, H. Chen, C. Zhou, *ACS Nano* 4 (2010) 4403-4411.
- [10]. P. C. Chen, G. Shen, S. Sukcharoenchoke, C. Zhou, *Appl. Phys. Lett* 94 (2009) 043113/1-043113/3.
- [11]. J. R. Miller, P. Simon, *Science*. Washington. DC. U. S 321 (2008) 651-652.
- [12]. C. Z. Yuan, L. Chen, B. Gao, L. H. Su, X. G. Zhang, *J. Mater. Chem* 19 (2009) 246-252.
- [13]. G. R. Li, Z. L. Wang, F. L. Zheng, Y. N. Ou, Y. X. Tong, *J. Mater. Chem* 21 (2011) 4217-4221.
- [14]. J. K. Chang, C. T. Lin, W. T. Tsai, *Electrochem. Commun* 6 (2004) 666-671.
- [15]. H. Subramanian, R. Vajtai, P. M. Ajayan, B. Wei, *J. Phys. Chem. B* 109 (2005)

20207-20214.

- [16]. K. C. Liu, M. A. Anderson, *J. Electrochem. Soc* 143 (1996) 124-130.
- [17]. C. Z. Yuan, B. Gao, L. H. Su, X. G. Zhang, *Solid State Ionics* 178 (2008) 1859-1866.
- [18]. Y. Y. Gao, S. I. Chen, D. X. Cao, G. I. Wang, J. L. Yin, *J. Power Sources* 195 (2010) 1757-1760.
- [19]. S. L. Xiong, C. Z. Yuan, X. G. Zhang, B. J. Xi, Y. T. Qian, *Chem.-Eur. J* 15 (2009) 5320-5326.
- [20]. M. R. Tarasevich, B. N. Efremov, S. Trasatti, Elsevier: USA 1982.
- [21]. X. Y. Liu, S. J. Shi, Q. Q. Xiong, L. Li, Y. J. Zhang, H. Tang, C. D. Gu, X. L. Wang, J. P. Tu, *ACS Appl. Mater. Inter* 5 (2013) 8790-8795.
- [22]. M. C. Liu, L. B. Kong, C. Lu, X. J. Ma, X. M. Li, Y. C. Luo, L. Kang, *J. Mater. Chem. A* 1 (2013) 1380-1387.
- [23]. L. Q. Mai, F. Yang, Y. L. Zhao, X. Xu, L. Xu, Y. Z. Luo, *Nat. Commun* 2 (2011) 1387/1-1387/5.
- [24]. W. W. Zhou, D. Z. Kong, X. T. Jia, C. Y. Ding, C. W. Cheng, G. W. Wen, *J. Mater. Chem. A* 2 (2014) 6310-6315.
- [25]. J. P. Liu, J. Jiang, C. W. Cheng, H. X. Li, J. X. Zhang, H. Gong, H. J. Fan, *Materials. Adv. Mater* 23 (2011) 2076-2081.
- [26]. L. Qian, L. Gu, L. Yang,; H. Y. Yuan, D. Xiao, *Nanoscale* 5 (2013)7388-7396.
- [27]. J. Xiao, S. Yang, *RSC Adv* 1 (2011) 588-595.
- [28]. J. Yan, Z. J. Fan, W. Sun, G. Q. Ning, T. Wei, Q. Zhang, R. F. Zhang, L. J. Zhi, F. Wei, *Adv. Funct. Mater* 22(2012) 2632
- [29]. X. Xia, W. Lei, Q. Hao, W. Wang, X. Wang, *Electrochim. Acta* 99(2013)253 - 261.
- [30]. Y. E. Roginskaya, O. Morozova, E. Lubnin, Y. E. Ulitina, G. Lopukhova, S. Trasatti, *Langmuir* 13(1997) 4621-4627.
- [31]. J. Marco, J. Gancedo, M. Gracia, J. Gautier, E. Ríos, F. J. Berry, *Solid State Chem* 153(2000) 74-81.
- [32]. J. H. Zhong, A. L. Wang, G. R. Li, J. W. Wang, Y. N. Ou, Y. X. J. Tong, *Mater.*

- Chem. 22(2012) 5656.
- [33]. X. Y. Liu, Y. Q. Zhang, X. H. Xia, S. J. Shi, Y. Lu, X. L. Wang, C. D. Gu, J. P. Tu, J. Power Sources 239 (2013) 157-163.
- [34]. X. Wang, X. D. Han, X. D. Lim, N. D. Singh, C. L. Gan, M. Jan, P. S. Lee, J. Phys. Chem. C 116 (2012) 12448-12454.
- [35]. B. Liu, J. Zhang, X. F. Wang, G. Chen, D. Chen, C.W. Zhou, G.Z. Shen, Nano Lett 12 (2012) 3005-3011.
- [36]. J. Yan, Z. J. Fan, W. Sun, G. Q. Ning, T. Wei, Q. Zhang, R. F. Zhang, L. J. Zhi, F. Wei, Adv. Funct. Mater. 22(2012) 2632-2641.
- [37]. Y. Y. Wei, S. Q. Chen, D. W. Su, B. Sun, J. G. Zhu, G. X. Wang, J. Mater. Chem. A 2 (2014) 8103-8109.
- [38]. G.X. Pan, X.H. Xia, F. Cao, P.S. Tang, H.F. Chen, Electrochem Commun 34 (2013) 146 - 149.



Scheme 1. Schematic illustration of the two-step synthesis of $\text{NiCo}_2\text{O}_4 @ \text{NiMoO}_4$ core/shell nanomaterials

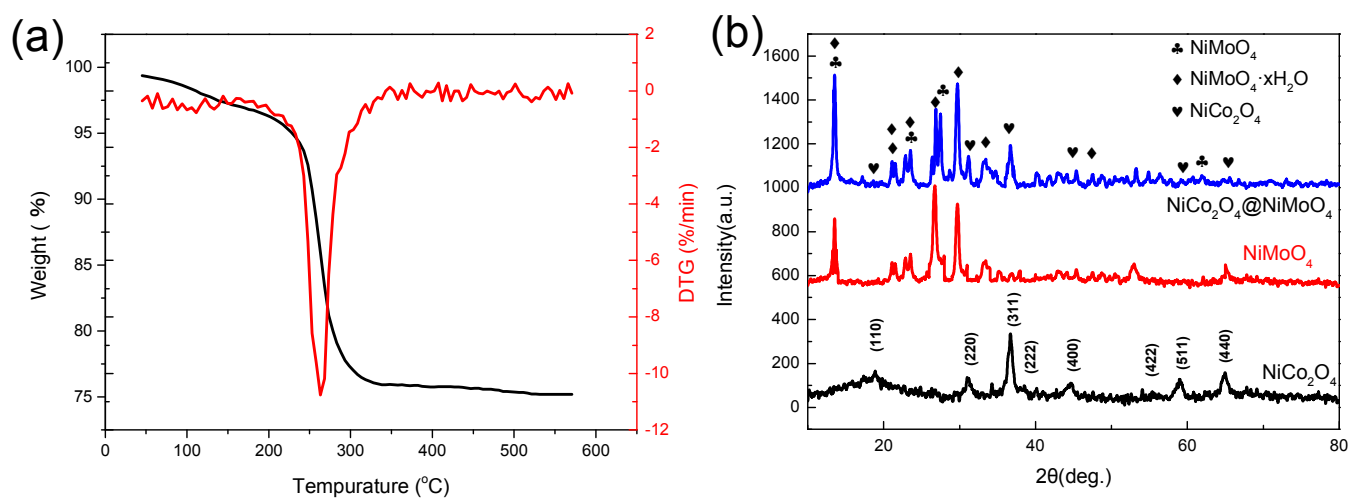


Fig.1(a) TG (black) and DTG (red) curves of NiCo_2O_4 **(b)** XRD patterns of backbone NiCo_2O_4 (black line) and hierarchical $\text{NiCo}_2\text{O}_4 @ \text{NiMoO}_4$ core/shell nanomaterials (red line)

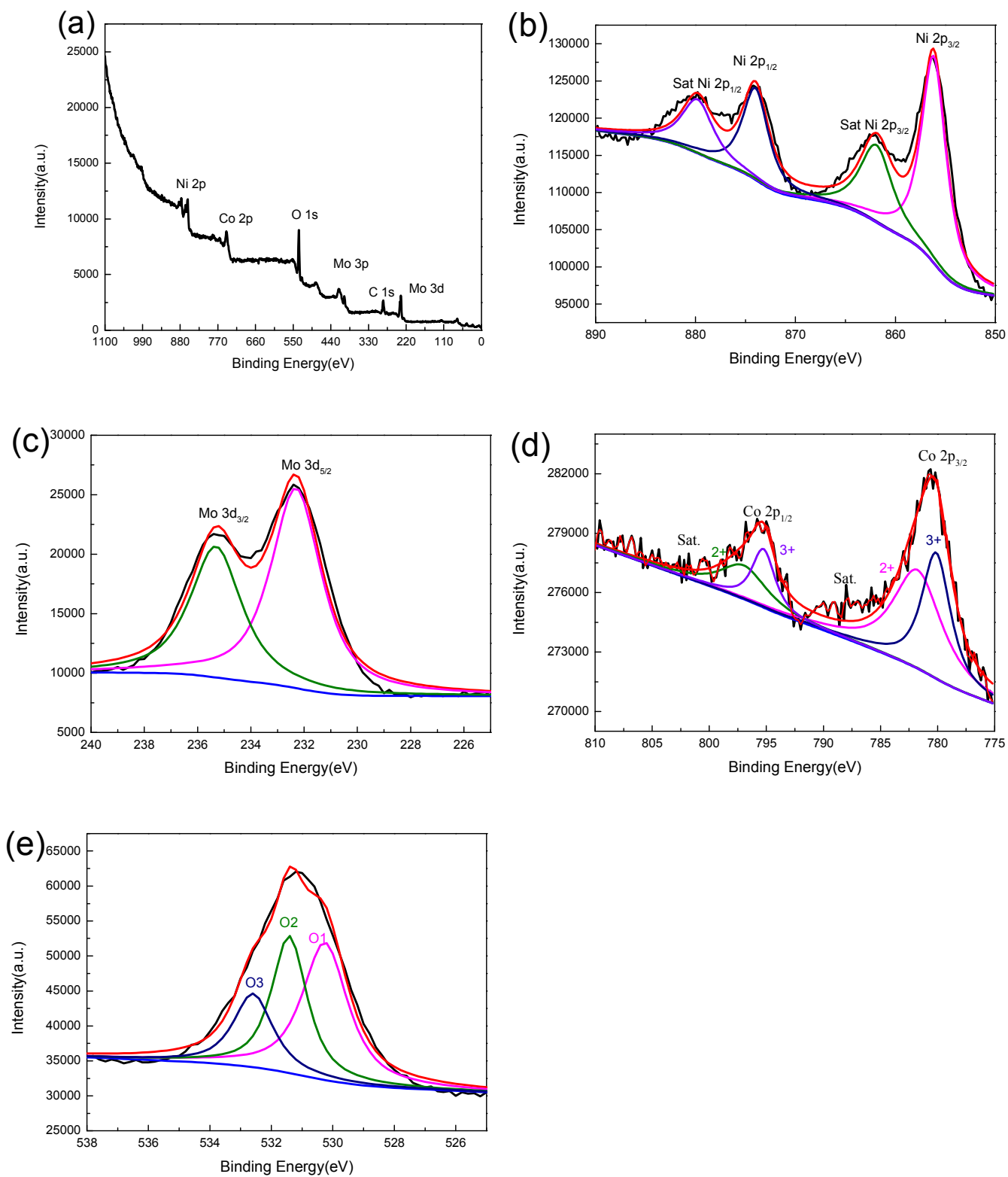


Fig. 2 XPS spectra of (a) survey spectrum, (b) Ni 2p, (c) Co 2p, (d) Mo 3d and (e) O 1s for seurchin-like $\text{NiCo}_2\text{O}_4@ \text{NiMoO}_4$ microspheres

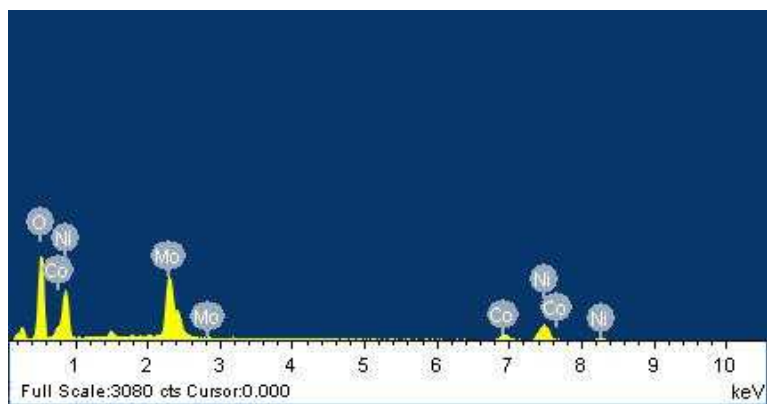


Fig.3 EDS analysis of the $\text{NiCo}_2\text{O}_4@ \text{NiMoO}_4$ core/shell nanomaterials

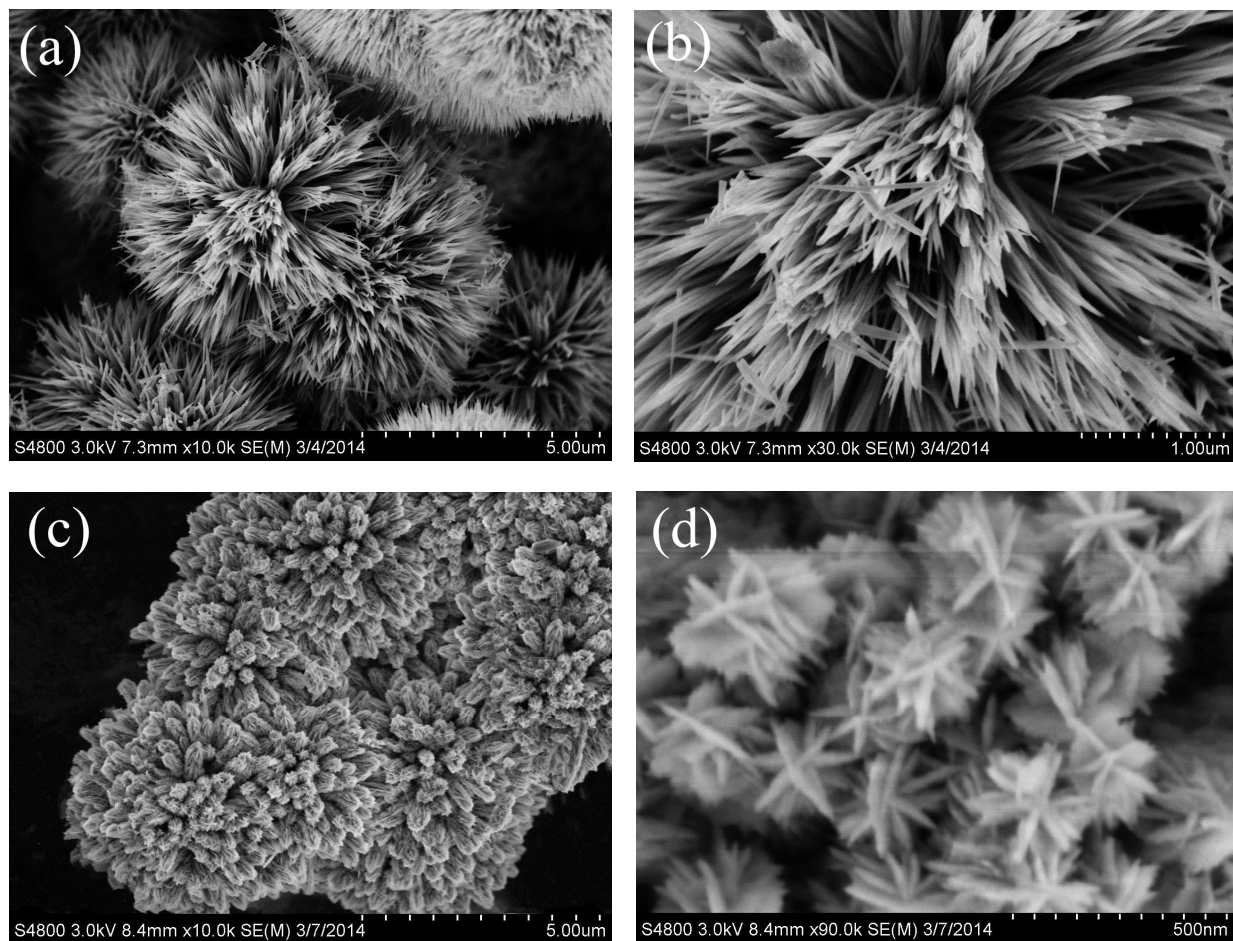


Fig. 4 (a,b) SEM image of the backbone NiCo_2O_4 nanostructures; (d,e,) SEM images of hierarchical $\text{NiCo}_2\text{O}_4@ \text{NiMoO}_4$ core/shell nanostructures

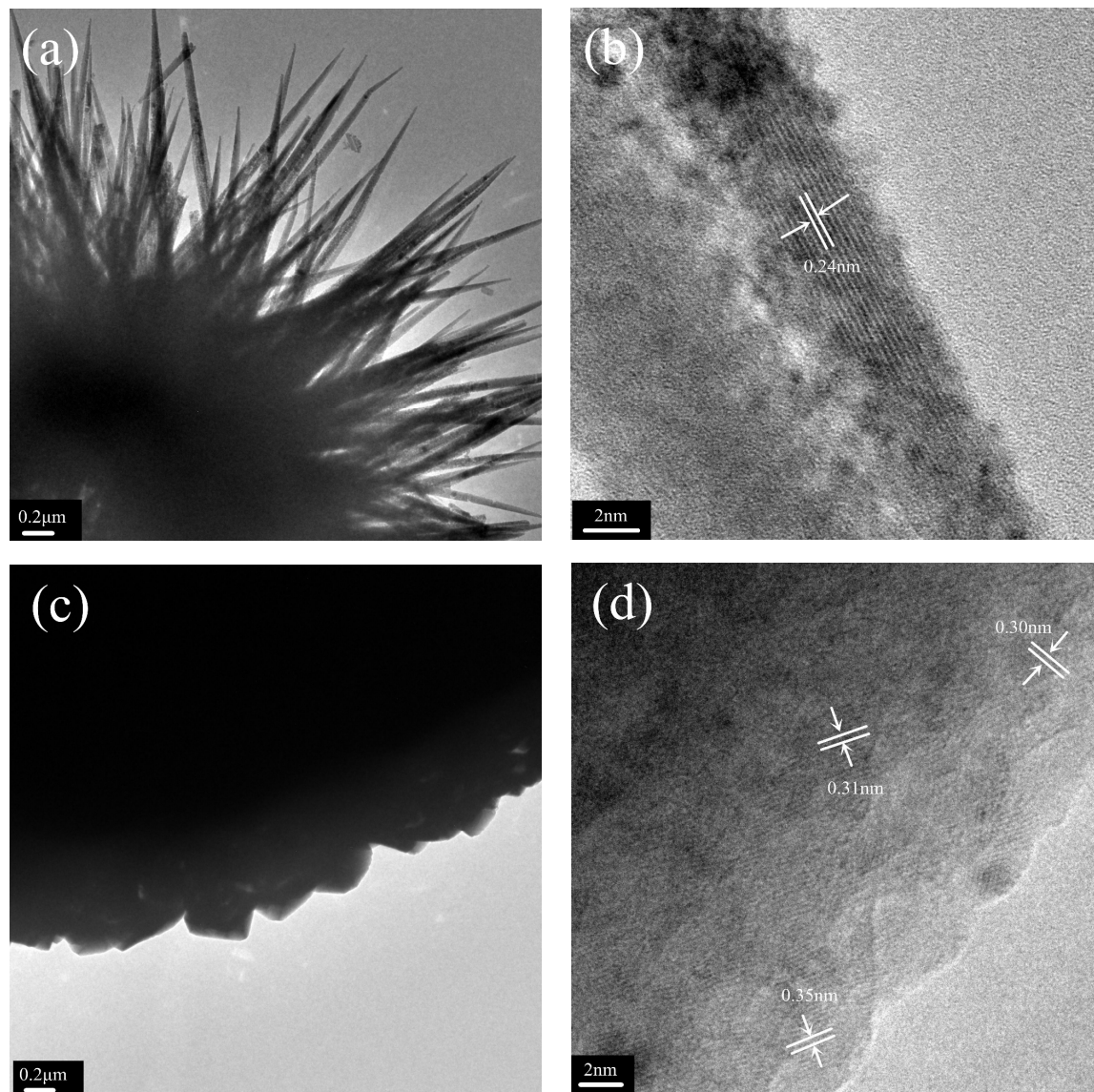


Fig. 5 (a) Low-magnification TEM image, (b) HRTEM image of NiCo_2O_4 nanostructures ; (c) low-magnification TEM image and (d) HRTEM image of the $\text{NiCo}_2\text{O}_4@ \text{NiMoO}_4$ core/shell nanostructures

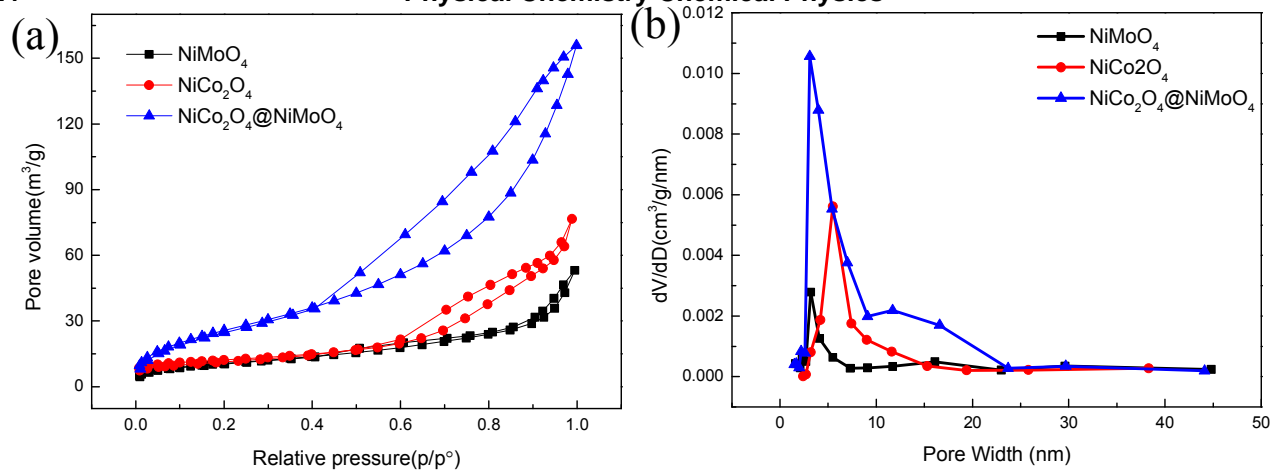


Fig.6 (a) N₂ adsorption/desorption isotherms (b) Pore size distribution of NiCo₂O₄, NiMoO₄ and NiCo₂O₄@NiMoO₄ core/shell nanomaterials

Table1. The specific surface area and total pore volume of the NiCo₂O₄, NiMoO₄ and NiCo₂O₄@NiMoO₄ samples

Sample	S _{BET} (m ² ·g ⁻¹)	V _{tot} (cm ³ · g ⁻¹)
NiCo ₂ O ₄	42.2	0.118
NiMoO ₄	39.2	0.080
NiCo ₂ O ₄ @NiMoO ₄	100.3	0.241

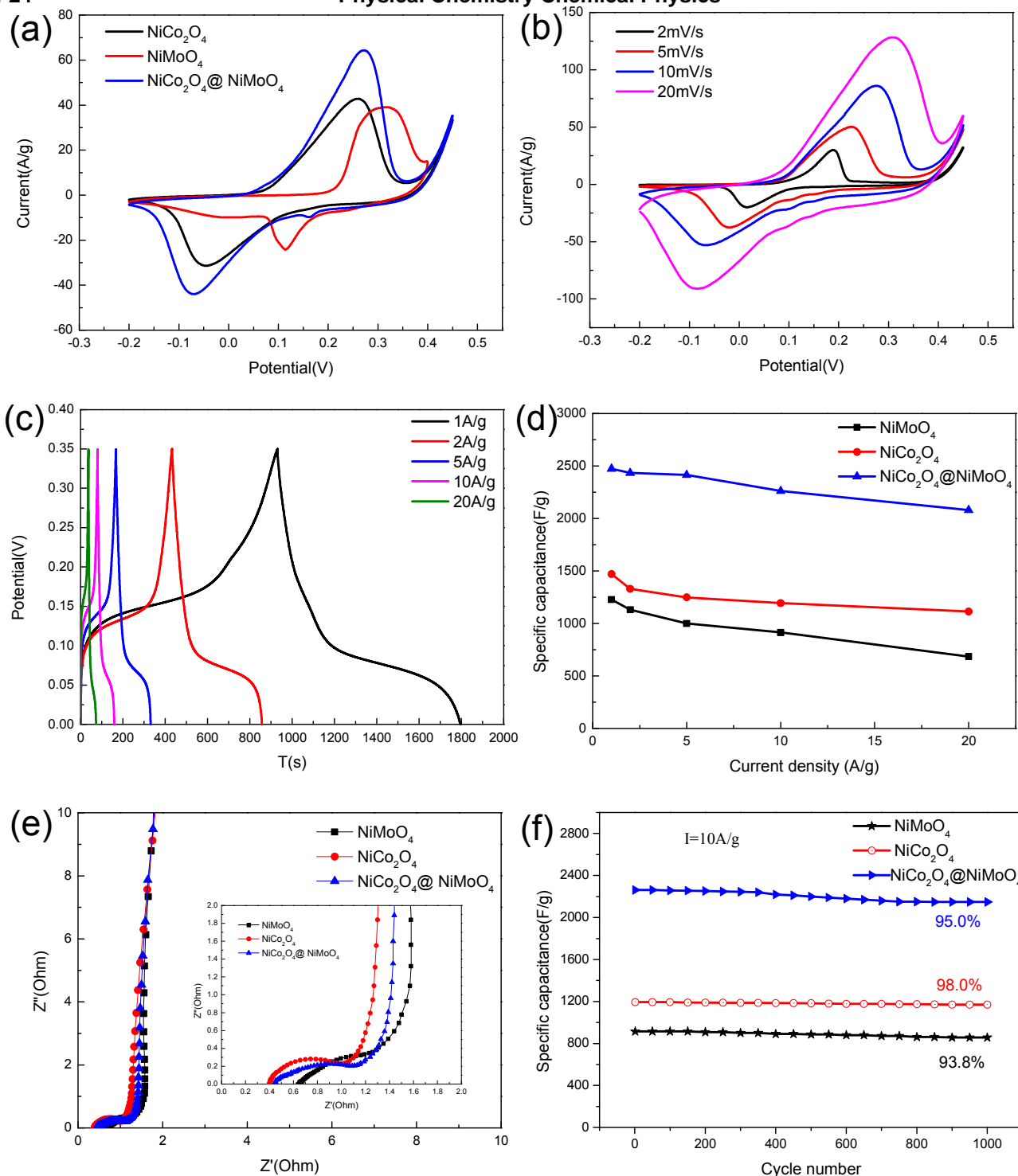


Figure 7. Electrochemical performances of NiCo₂O₄, NiMoO₄ and NiCo₂O₄@NiMoO₄ electrodes: (a) comparative CV curves recorded at a scan rate of 10 mV s⁻¹ for the three different electrodes; (b) CV curves at different scan rates for NiCo₂O₄@NiMoO₄ electrode; (c) charge-discharge curves at different current densities of NiCo₂O₄@NiMoO₄ electrode; (d) specific capacitance as a function of discharge current density; (e) AC impedance plots of three electrodes; (f) variation of specific capacitance with cycle numbers at a current density of 10 A g⁻¹

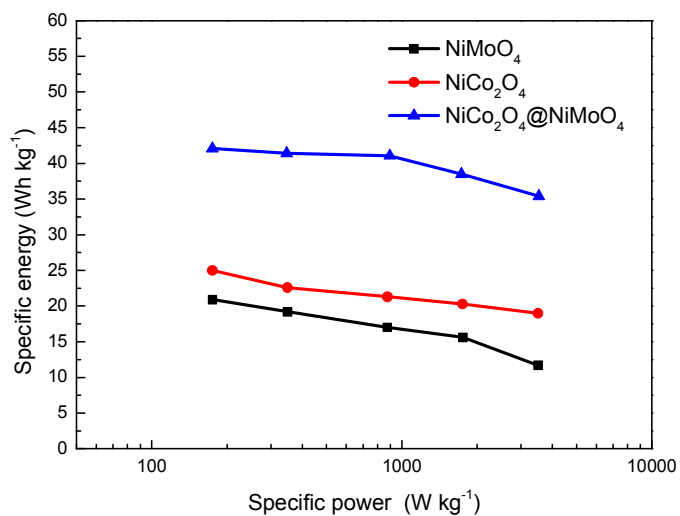


Fig. 8 Ragone plot of the estimated specific energy and specific power at various charge - discharge rates.